KECK Geology Consortium
Learning Science Through Research
Published by the Keck Geology Consortium
Short Contributions
Keck Geology Consortium
Volume 37
May 2025
doi: 10.18277/AKRSG.2025.37.05

ANALYZING FRACTURE CHARACTERISTICS IN THE LOW DISPLACEMENT ZONE ON THE SPENCER BENCH SEGMENT OF THE SEVIER NORMAL FAULT, SOUTHWEST UTAH

ARIEL MONTALVO, Whitman College
Project Advisor: Gui Aksit

INTRODUCTION

Understanding fault dynamics and characteristics as faults propagate and accumulate displacement is important in the development of natural resources and seismic hazard assessment. Geologists have established that during the propagation of a fault, an envelope forms around the fault plane due to local stresses, creating minor faults and intense fracturing in a damage zone (e.g., Peacock and Sanderson, 1996; Shipton and Cowie, 2003; Kim et al., 2004; Choi et al., 2016). We study these damage zones to help us understand fracturing and faulting in the rock, which can increase permeability, groundwater flow rates (e.g., Rowlety,1998), hydrocarbon migration (e.g., Morely et al, 1990), ore mineralization (e.g., DeWitt et al., 1986), and geothermal energy production potential (e.g, Siler et al., 2018; Neath and Surpless, 2022; Jennings and Surpless, 2023).

In this project, I aimed to better understand fracture characteristics in the Spencer Bench segment of the Sevier normal fault in Southwest Utah, located within Red Hollow Canyon near the town of Orderville, Utah (Fig. 1). A combination of ground-based scanline surveys from previous years was used in addition to Structure from Motion (SfM) modeling (e.g., Johnson et al., 2014) to collect and analyze fracture data within the study area. Data include fracture intensity and orientation of fractures relative to the fault surface. In this study area, the fault displays low dip-slip displacements (~10 m in the north tapering to ~3 m in the south) compared to other segments of the fault zone, and it shares the same lithologies in the hanging wall and footwall, permitting us to hold lithology constant in our analysis of the fracture network.

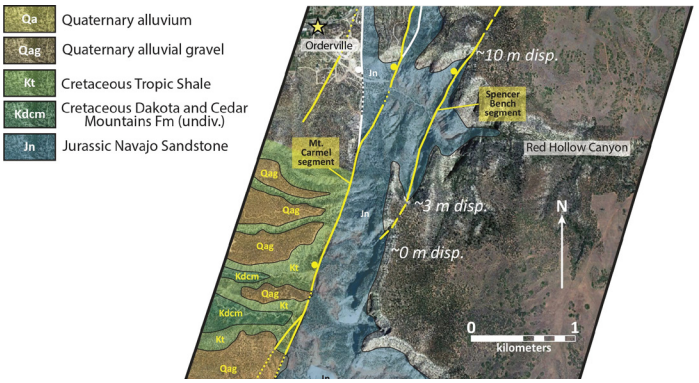

Figure 1. Overview map of the study area showing lithology and the right stepping en echelon fault segments, including the Spencer Bench to the east of the town of Orderville, Utah. Displacement is shown in Red Hollow Canyon, where the Structure-from-Motion (SfM) model was built.

BACKGROUND

The Sevier normal fault is located within the transition between the Basin and Range province to the west and the Colorado Plateau to the east (see Fig. 1 in Surpless, this volume). Here, normal faulting accommodates extension from the Basin and Range, and the Sevier fault shares characteristics of both geologic provinces. The Sevier fault has a surface trace of 100 km, and its segments broadly trend northeast (e.g., Reber et al., 2001). The fault is steeply west dipping, and dip-slip displacement in the study area is ~400-800 m (e.g., Taylor et al.,2024). The Sevier fault is made up of numerous right-stepping en echelon segments.

This project focused on the Spencer Bench fault segment, near the town of Orderville, Utah, where the segment is the easternmost extent of the right-stepping fault network. To the west is the Mt Carmel Segment, and further west of that is the Orderville segment, which nearly bisects the town of Orderville, striking north-south (Fig. 1). The lack of vegetation and

access to outcrops provide opportunity to document the evolution of the fault and fault damage zone characteristics. Both the hanging wall and footwall are the Jurassic Navajo Sandstone. This allows us to compare the north to south portions of the fault where it is exposed within Red Hollow Canyon and to document fracture characteristics in the hanging wall and footwall of the fault.

METHODS

For this project, there were various methods for data collections and data analysis. These include: field data collection for fracture scanlines, the construction of a 3D structure-from-motion (SfM) model based on drone-based image capture for areas that were not accessible on foot, and the analysis of the field scanlines and scanlines from the 3D model to interpret fracture characteristics. This project compares fracture orientation and intensity from the north to the south, in addition to the hanging wall versus the footwall of the fault.

Field Data Collection

Data were collected on well-exposed and continuous outcrops by documenting the position of fractures along scanlines that were oriented perpendicular to fracture strike. Fractures documented were at least three meters long, and scanline location start and end points were recorded by GPS coordinates. The use of Brunton compasses along with a tape measure allowed for the measurement of fracture orientation and spacing in relation to the fault plane for a given outcrop. These structural measurements along with other notable structures such as slickenlines or locations of interest were recorded along with detailed notes, sketches and photographs as supplementary data.

3D Model Construction

In locations that were not accessible due to terrain restrictions, a DJI Mavic 3 unmanned aerial vehicle was flown to record high quality video footage that could be used to build a model. Using VLC Media Player, we extracted still images from these videos which provide overlapped images that can be used to build a model. These images were used with Agisoft Metashape Professional along with Google Earth to construct a spatially correct and georeferenced Structure from Motion model which was used for further data collection and analysis. Images with 60-80% overlap were aligned to create a point cloud distributing images into 3D space. To ensure that the model was spatially correct, a digital elevation model was marked using latitude, longitude and elevation. Once this was done, the model was ready to be made into a high resolution, high definition and spatially correct orthomosaic which could be used for data collection.

Analysis of Field Data

Using the data collected in the field, fracture intensity was calculated as a number of fractures per meter. Fracture spacing was calculated as the modified coefficient of variation, $Cv'=\sigma/M$, a new measure of fracture clustering recently developed by Hooker et al. (2023). In this equation, σ = the standard deviation of fracture spacing, and M = the median fracture spacing along a given scanline. Stereonet software (Allmendinger, 2024) was used to create projections of fracture orientation data and to compare data in the footwall to that in the hanging wall.

Analysis of 3D Model

Once the model was completely built, software markup tools enabled the creation of digital scanlines that were established perpendicular to fault or fracture strike, just as ones in the field were. Because the model is spatially accurate, using the measuring tool in Agisoft provided data of fracture intensity and orientation the same as that from the field. These data were also used to calculate Cv' (Hooker et al., 2023) and to plot stereonets comparing the different sides and segments of the Spencer Bench segment. It is important to note that given the resolution and scale of the model, some fractures are not easily documented, making it difficult to compare data collected from the model to ground-based scanlines.

RESULTS

Scanline data collected from the 3D computer model are limited to the hanging wall in both northern and southern exposures due to a lack of visible fractures in

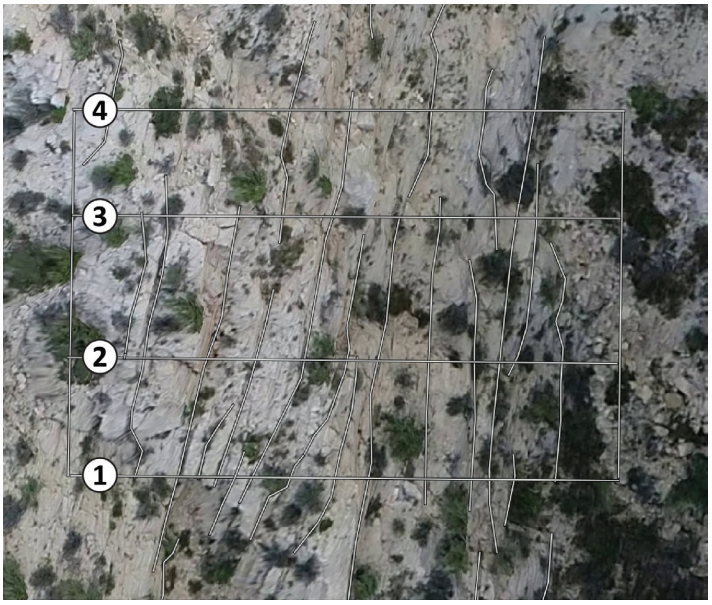

Figure 2. Scanline framework for fracture analysis in the northern section (hanging wall) of the model. Fracture intensity (number of fractures/length of scanline) ranged from ~0.20 m^{-1} to ~0.45 m^{-1}.

the footwall. Model analysis reveals that fractures on the hanging wall are oriented sub-parallel to the fault plane in both northern and southern exposures within Red Hollow Canyon (Figs. 2 and 3). Scanline analysis of these exposures reveals a greater average fracture

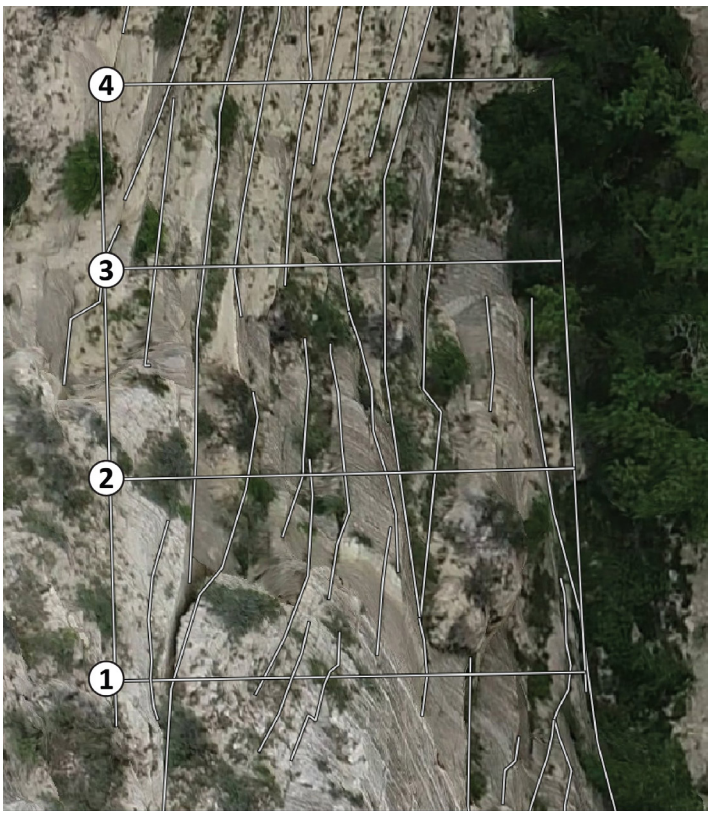

Figure 3. Scanline framework for fracture analysis in the southern section (hanging wall) of the model. Fracture intensity (number of fractures/length of scanline) ranged from ~0.61 m^{-1} to ~0.77 m^{-1}.

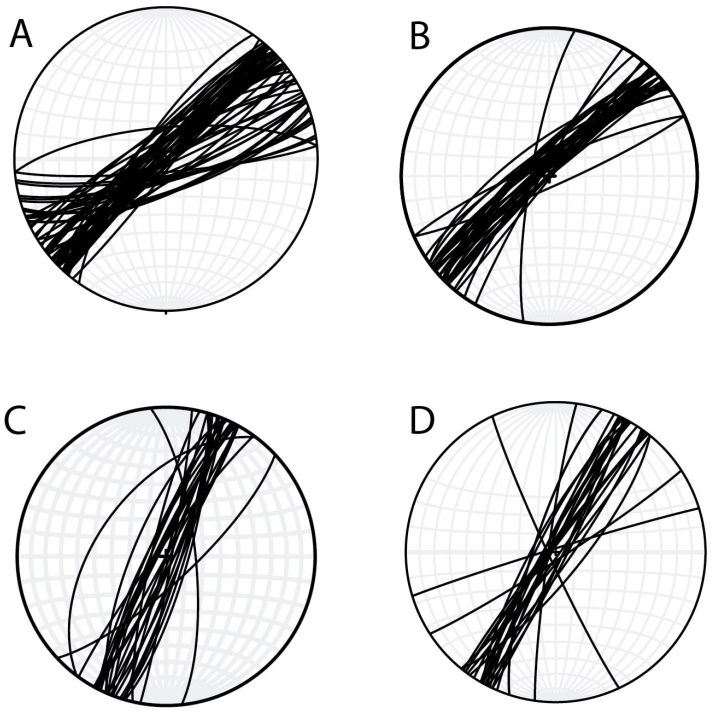

Figure 4. Stereonet equal-area lower-hemisphere projections showing orientations of ground-based scanlines on both sides of the fault. A) Footwall-North central; B) Footwall-Central; C) Hanging Wall- Central; and D) Hanging Wall- South central.

intensity where fault displacement is three meters in the south (Fig. 3) as compared to the northern exposure where it is 10 meters (Fig. 2). The northern exposure fracture intensity ranged from 0.2 - 0.45 m^{-1}, whereas the southern exposure showed higher values, from 0.61 - 0.77 m^{-1}. This suggests that increasing dip-slip displacement does not necessarily result in a greater fracture intensity. However, more fracture data are needed to substantiate the relationship between displacement magnitude and fracture intensity.

In addition, ground-based scanline data reveal that fracture intensity values are much higher in the hanging wall (0.97 - 1.27 m^{-1}) relative to the footwall (0.33 - 0.34 m^{-1}). These data are consistent with previous research that suggests asymmetry in normal fault damage zones (e.g., Berg and Skar, 2005; Liao et al., 2022; Jennings and Surpless, 2023). Because strain-related fracturing propagates in an orientation that is more energetically favorable based on fault propagation direction (e.g., Sharon and Fineberg, 1996; Zhou et al., 2018; Fineberg and Bouchbinder, 2015; Surpless and McKeighan, 2022), so this asymmetry is best explained by the upward propagation of displacement, which results in greater hanging wall damage relative to the footwall.

Ground-based scanline data also show that fracture orientations in the hanging wall are sub-parallel to the fault plane, while footwall fractures strike at an acute angle of approximately 25 degrees clockwise relative to the fault plane (Fig. 4). Lithology on both sides is the same, and thus a possible explanation for the angle of these fractures could be a strike slip element affecting the sandstone on the footwall, where the fault acts to isolate the stress field in the hanging wall relative to the footwall (e.g., Surpless and McKeighan, 2022). However, more research is required to explain this abrupt spatial change in fracture orientation.

ACKNOWLEDGEMENTS

Funding for this project was provided by a 2024-2025 Keck Geology Consortium Advanced Research Project Grant as part of an NSF-REU Award to the Keck Geology Consortium. (EAR 1659322; Pls Wirth, K., and Davidson, C.) Funding was also provided by SNF Award 2042114 to PI Surpless and by the Trinity University Department of Earth and Environmental Geosciences. I would like to personally thank Ben Surpless for his help and guidance throughout the field season in the summer until the very end of this project. I would also like to thank and acknowledge Gui Aksit, my on campus project advisor for all of her help and support throughout this. Lastly, I want to thank Kirsten Nicolaysen for her guidance, advice, and help in applying for this REU.

REFERENCES

Allmendinger, R., 2024, Stereonet computer software, v. 11, accessed 2024.

Berg, S.S., and Skar, T., 2005, Controls on damage zone asymmetry of a normal fault zone: outcrop analyses of a segment of the Moab fault, SE Utah: Journal of Structural Geology, v. 27, pp. 1803–1822, doi:10.1016/j.jsg.2005.04.012.

Choi, J-H., Edwards, P., Ko, K., and Kim, Y-S., 2016, Definition and classification of fault damage zones: a review and a new methodological approach: Earth Science Reviews, v. 152,

Cowie, P.A., and Shipton, Z.K., 1998, Fault tip displacement gradients and process zone dimensions: Journal of Structural Geology, v. 20, n. 8, pp. 983-997.

Fineberg, J., and Bouchbinder, E., 2015, Recent developments in dynamic fracture: Some perspectives, International Journal of Fracture, v.196, 33 – 57

Hooker, J., Marrett, R., and Wang, Q., 2023, Rigorizing the use of the coefficient of variation to diagnose fracture periodicity and clustering: Journal of Structural Geology, doi: 10.1016/j.jsg.2023.104830.

Kim, Y., Peacock, D.C., and Sanderson, D.J., 2004, Fault damage zones: Journal of Structural Geology, v. 26, pp. 503-517, doi:10.1016/j.jsg.2003.08.002.

Mayolle, S., Soliva, R., Dominguez, S., Wibberley, C., 2023, Normal fault damage zone growth in map view from analogue models: Journal of Structural Geology, v. 176, doi:10.1016/j.jsg.2023.104975

McGrath, A.G., and Davidson, I., 1994, Damage zone geometry around fault tips: Journal of Structural Geology, v. 17, no. 7, pp. 1011-1024.

Peacock, D.C.P., and Sanderson, D.J., 1996, Effects of propagation rate on displacement variations along faults: Journal of Structural Geology, v. 18, p. 311 –320.

Reber, S., Taylor, W.J., Stewart, M., and Schiefelbein, I.M., 2001, Linkage and reactivation along the northern Hurricane and Sevier faults, southwestern Utah: Utah Geological Association

Sharon, E., Fineberg, E., 1996, Microbranching instability and the dynamic fracture of brittle materials: Physics Reviews, v. B54, p. 7128–7139.

Shipton, Z., and Cowie, P., 2003, A conceptual model for the origin of fault damage zone structures in high-porosity sandstone: Journal of Structural Geology, v. 25, p. 333-344

Taylor, W., Surpless, B., and Schiefelbein, I., 2024, Complex segment linkage along the Sevier normal fault, southwestern Utah: Lithosphere, doi: 10.2113/2024/lithosphere_2023_332.

Zhou, S., Zhuang, X., Zhu, H., Rabczuk, T., 2018, Phase field modeling of crack propagation -Branching Coalescence Rocks: Theoretical Applications of Fracture Mechanics, v. 96, p. 174–192.